THE JOURNAL OF PHYSICAL CHEMISTRY B

Article

pubs.acs.org/JPCB

# Photochromic Solid Materials Based on Poly(decylviologen) Complexed with Alginate and Poly(sodium 4-styrenesulfonate)

Luis Sanhueza,[†] Joaquín Castro,[†] Esteban Urzúa,[†] Lorena Barrientos,[§,∥] Felipe Oyarzun-Ampuero,[⊥] Héctor Pesenti,[‡] Toshimichi Shibue,[#] Natsuhiko Sugimura,[#] Wataru Tomita,[%] Hiroyuki Nishide,[%] and Ignacio Moreno-Villoslada*[,†]

[†]Instituto de Ciencias Químicas, Facultad de Ciencias, and [‡]Instituto de Materiales y Procesos Termomecánicos, Universidad Austral de Chile, Casilla 567, Valdivia, Chile

[§]Departamento de Química, Facultad de Ciencias Básicas, Universidad Metropolitana de Ciencias de la Educación, Avenida José Pedro Alessandri 774, Ñuñoa, Santiago, Chile

[∥]Center for the Development of Nanoscience and Nanotechnology, CEDENNA, Santiago, Chile

[⊥]Department of Science and Pharmaceutical Technology, Universidad de Chile, Santiago, Chile

[#]Materials Characterization Central Laboratory, School of Science and Engineering, and [%]Department of Applied Chemistry, Faculty of Science and Engineering, Waseda University, Tokyo 169-8555, Japan

**ABSTRACT:** Photochromic solid materials based on the cationic polymer poly(decylviologen) are reported. The solids were obtained by freeze-drying colloidal suspensions of nanocomplexes obtained by mixing aqueous solutions of the polycation with different solutions of polyanions such as poly(sodium 4-styrenesulfonate) or sodium alginate, at a cationic/anionic polymeric charge ratio of 0.7. The photochromic responses of the solid materials fabricated with alginate as complementary charged polyelectrolyte of the cationic polyviologen are faster than those of the solid materials fabricated with poly(sodium 4-styrenesulfonate), achieving coloration kinetics in the order of minutes, and discoloration kinetics in the order of hours for the former. Aromatic−aromatic interactions between the latter polyanion and the polyviologen may stabilize the dicationic form of the viologen derivative, increasing the necessary energy to undergo photoreduction, thus decreasing the reduction kinetics.

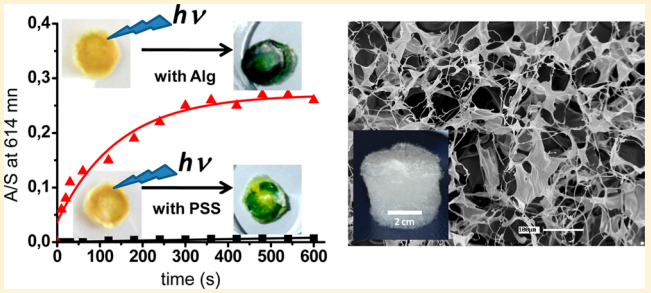


## 1. INTRODUCTION

*N*,*N*′-Disubstituted-4,4′-bipyridinium derivatives, also known as viologens, have been widely investigated due to their interesting photophysical[1−3] and electrochemical properties,[4−6] with potential technological applications in rechargeable batteries,[7] solar cells,[8−10] and electrochromic devices.[11,12] In this context, great interest has been devoted on the totally reversible redox process between the pale yellow dication and the deep violet radical cation states.[13] Related polymeric viologen derivatives can be easily prepared by the Menshuktin reaction, mixing equimolar amounts of 4,4′-bipyridine and desired dihaloalkanes.[14,15] The resulting polymers are dicationic in their natural state, thus also water-soluble. The solubility in water of these polymers may constitute a drawback when they must be immobilized in different solid devices, such as electrochromic devices or solid catalysts.[12,16,17]

The colorless dication state of viologens can be also switched to the respective colored radical cation state by a photoinduced reduction. This process involves the promotion of an electron from the counterion and derives in a change on the molecular structure of the viologen unit.[18,19] In order to obtain improved photochromic responses, some efforts have been made to attain a rapid photoswitching and control the lifetime of the colored radical cation state.[20] In general, it can be found that an ideal photochromic material must present good photoswitching in terms of reversibility and control of the kinetics of the color exchange between both redox states.[21,22] The modulation of the photochromic response regarding viologen renders these compounds as important materials to be applied in photoreduction of water,[1,23] as oxygen sensors,[24] electrooptical devices,[25] erasable photomemory,[26] etc. Several variables may affect the photoreduction process, involving the nature of the counterion, crystallinity of the samples, and the nature of the medium where viologens are embedded.[27] The nucleophilic character of the counterions has been established as an important factor to modulate the photoresponse of viologens;[28,29] in addition, the electron transfer from the counterions to the bipyridinium molecule is enhanced if ion pairs between the viologens and naked counterions are held. In this sense, humidity reduces the photoreduction, probably due

**Received:** June 22, 2015
**Revised:** September 17, 2015
**Published:** September 23, 2015





DOI: 10.1021/acs.jpcb.5b05963
*J. Phys. Chem. B* 2015, 119, 13208−13217

to the breakdown of the ion pairs through solvation, and therefore stabilizing the charges of both the viologen and the counterion, decreasing the energy of the oxidized form of the viologen.[29] In the solid state, the photoreduction of viologens are considerably enhanced when embedded in a dried polar aprotic polymeric matrix such as poly(vinylpyrrolidone) (PVP), whereas protic matrices such as poly(vinyl alcohol) (PVA) produce a decrease on the photoresponse.[26,27,29] It has been reported that isotropic materials resulted more photosensitive than similar anisotropic materials, mainly due to the shorter distances between the bipyridinium residue and the counterion, making easier the transfer of an electron upon irradiation.[30−32]

Counterions as electron donating agents include halides,[29] aromatic molecules with sulfonate groups,[32,33] and inorganic clusters.[25,34,35] In the particular case of hybrid systems based on organic viologens and inorganic clusters, the latter are used as electron donor moieties, playing, in addition, an important role on the modulation of the network topologies and the physical properties of these photochromic materials.[34,35] As an effective strategy to enhance the photoresponse, viologens have been also included in host−guest or interlocked complexes, where the macrocycle host has the electron-donating property, including $\pi$-electron-donating groups.[24,36] Among the macrocycles used, cyclodextrins,[37] benzocrown ethers,[36] and catenanes[38] can be found. Macrocyclic viologen derivatives may also be synthesized that act as hosts of $\pi$-electron-donating molecules such as dimethoxybenzene and indole, producing modulation of the resulting color after the photochromic reaction.[39]

Color fading may take place in the dark through thermal back electron transfer from the radical cation to a counter radical anion or through oxidation of the radical cation in the presence of molecular oxygen. Discoloration in the dark may consume several days or even months. Sulfonate-modified viologens are shown to last for at least one year in its reduced state in the air.[33] In the particular case of host−guest complexes between viologens and benzocrown ethers, it has been shown that the faster kinetics of the bleaching process is consistent with the stabilization energy of the complex between the donor host molecule and the dication viologen, compared to the energy of the complex with the radical cation.[36] Differences in the discoloration kinetics are reported to be a function of the structural arrangements between viologens and their counterparts when they are inserted in polymer matrices.[32] The matrix in which viologens are embedded may have an active role in the stabilization of the colored material, since may reduce oxygen and water permeability.[27,28] Examples of materials containing viologen derivatives are reported showing color fading by $O_2$ that are considered fast (from minutes to hours)[35,40] and very fast (within 5 s).[24]

Different photochromic materials have been made using viologens, such as organic films, crystals, and porous materials. Photochromic porous materials have been mainly based on metal−organic frameworks (MOFs).[24,41,42] Porous crystalline chemical sensors are quite interesting because of their quick, reversible, and recyclable sensing ability. In addition to sensing applications, porous materials containing viologens may be used as catalysts, adsorbents, and ion exchangers. In this context, freeze-drying, also known as lyophilization, appears as a suitable technique to obtain micro- and/or nanoporous matrices. Sophisticated structures are explained under the scope of the "ice-segregation-induced self-assembly" (ISISA) framework.[43,44] In the first step of this process, solutions are frozen for a determined period of time in order to obtain water crystals. During freezing, solute molecules that were originally isotropically dispersed are displaced to the boundary edges between adjacent hexagonal crystals of ice. In the second step of the process, sublimation of ice gives rise to a microporous material, characterized by a frame of matter, with empty spaces that originally were occupied by the ice crystals. By accurately controlling the experimental conditions of the freezing step, a huge range of morphological structures, including aligned[43,45] or nonaligned[46] structures, can be obtained. The importance of ISISA on the control of morphological properties of materials has been evidenced using a wide range of low- and high-molecular-weight molecules, including organic and inorganic compounds.[44,46,47]

Water-insoluble interpolymer complexes may be obtained by mixing polyviologens with several water-soluble polyanions, so that Coulombic interactions are held. In particular, poly(sodium 4-styrenesulfonate) (PSS) has shown to produce macrometer-sized polymer complexes with poly(decylviologen) (PV10) that have been satisfactorily included in several technological devices.[12,15,48] Sodium alginate (Alg) is another interesting polyanion to be used. The structure of Alg is based on $\beta$-D-mannuronate and $\alpha$-L-guluronate, covalently linked together in different sequences or blocks. Alg-derived complexes are often nontoxic, biocompatible, and cheap, so that they have been successfully applied for oral delivery of drugs,[49,51] cell encapsulation,[52,53] and nutrient carriers in food industry.[50,54] Polyelectrolyte complexes such as chitosan−Alg[49] and pectin−Alg[50] have been studied and applied as pH-sensitive hydrogels and food carriers, respectively. In order to prevent macroprecipitation of interpolymer complexes, colloidal suspensions of nanoparticles may be formed by accurately choosing the total amount and relative concentration of each component. Nanocomplexes provide both a close contact between reacting species and stability of the aqueous suspensions. This last property is desirable to allow a suitable molecular distribution during formation of ice crystals when the suspensions are submitted to freeze-drying.

In this paper, the obtention of totally organic, photochromic porous materials based on PV10 as photoactive compound is shown. The materials are obtained by freeze-drying suspensions of nanocomplexes of PV10 as polycation and PSS or Alg as polyanion. The resulting materials have a porous structure similar to sugar-cotton sponges. Mechanical pressure on the sponges provides tougher materials with a structure similar to starch wafers. Interactions between molecules have been analyzed by $^1$H NMR. The nanostructured PV10/polyanion suspensions have been analyzed by dynamic light scattering (DLS) and scanning transmission electron microscopy (STEM). UV−vis spectroscopy, scanning electron microscopy (SEM), and X-ray diffraction (XRD) techniques have been used to characterize the materials. The photochromic properties of the resulting materials, including coloration and discoloration kinetics, are finally studied.

## 2. EXPERIMENTAL SECTION

**2.1. Reagents and Solvents.** Commercially available reagents and solvents were used without further purification. Poly(sodium 4-styrenesulfonate) (PSS, $M_W$ = 70 000 g/mol, Sigma-Aldrich) and sodium alginate (Alg, EncapBioSystems Inc.) were used as polyanions. Poly(decylviologen) (PV10) was synthesized by previously reported methods.[55] Briefly, equimolar amounts of 4,4′-bipyridine and 1,10-dibromodecane


DOI: 10.1021/acs.jpcb.5b05963
J. Phys. Chem. B 2015, 119, 13208−13217

were dissolved in 5 wt % of dried acetonitrile, and the mixture was stirred and heated at 80 °C for 72 h. The resulting yellow precipitate was filtered, washed with small amounts of acetonitrile, followed by small amounts of acetone, and then dried at 60 °C. The length of the polymer chain was confirmed by $^1$H NMR experiments and achieved 15 units. $D_2O$ (Acros) was used for $^1$H NMR sample preparation. $NaBH_4$ (Merck) was used for chemical reduction. The molecular structures of the polymers are shown in Figure 1. Aqueous solutions were prepared in deionized water (18.2 MΩ).

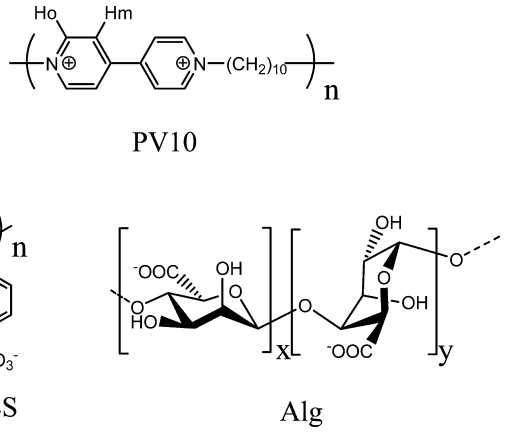


**Figure 1.** Molecular structures of PV10, PSS, and Alg.

**2.2. Equipment.** Deionized water showing 18.2 MΩ of resistance was obtained in a Simplicity Millipore deionizer. UV−vis measurements of solid samples were performed in a UV-2600 Shimadzu spectrophotometer by diffuse reflectance experiments. $^1$H NMR measurements were made in JNM-Lambda 500 (JEOL, 500 MHz) and AVANCE 600 spectrometer (Bruker, 600 MHz) spectrometers. Apparent size and zeta potential of the colloidal suspensions were obtained in a Malvern Zetasizer Nano ZS (Malvern) instrument with backscatter detection (173°), controlled by the Dispersion Technology Software (DTS 6.2, Malvern). STEM images were obtained in an Inspect 50 (FEI) instrument. Lyophilized samples were prepared in a Christ, Alpha 1-2 LD plus lyophilizer. SEM images were obtained in an S-4500 S field emission-scanning electron microscope (HITACHI). XRD patterns were obtained in a BRUKER D2 phaser diffractometer with a LYNXEYE detector. A stainless steel piston of three pieces was used for pressing the sponges. The piston consisted of (see Figure 2): (1) a hollow cylinder of 2.5 cm of lumen and 1 cm of wall thickness, including a thread in the internal face of one of its ends; (2) a base with external thread matching that of the cylinder; and (3) a massive cylinder of 2.5 cm diameter, matching the hollow cylinder lumen, and 5 cm of length, with a nondetachable base at one end. Wafers were obtained in a hydraulic press CARVER, model 3851-OC, with pressing limit of 11 tons.

**2.3. Procedures.** *Polymer Solution Preparation.* Solutions of PSS and/or PV10 have been prepared in $H_2O$ or $D_2O$. Conventional and well-known procedures have been followed. Particular experimental conditions are provided in the figure captions. $^1$H NMR spectra were obtained in $D_2O$ at 298 K.

*Nanoparticle Suspensions Preparation.* In order to prepare the nanoparticle suspensions, mixtures of both anionic and cationic polymers were prepared at a final concentration of

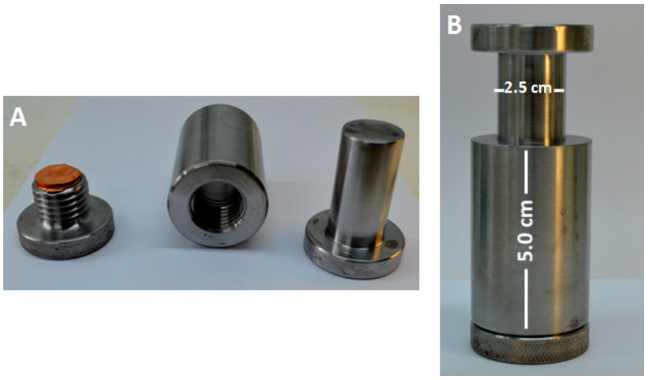


**Figure 2.** Stainless steel piston configuration. (A) Piston parts and sponges gently pressed between copper plates before assembling the pieces. (B) The piston parts are mounted with the sponges and copper plates inside before pressing under 5 tons.

total polymeric ionic groups ($n_T = n^+ + n^-$) of $8 \times 10^{-3}$ M, considering the number of polymeric anionic groups ($n^-$) and cationic groups ($n^+$), from stock solutions of $2 \times 10^{-2}$ M of each polymer. The mixing volumes of anionic and cationic polyelectrolytes have been chosen in order to provide formulations showing $n^+/n^-$ in the range between 0.1 and 2.0. Samples were analyzed by photon correlation spectroscopy and laser Doppler anemometry measured at 173° and 298 K, obtaining the apparent hydrodynamic diameter and the zeta potential of the nanoprecipitates, respectively. Each measurement including size and zeta potential was done in triplicate. STEM images where obtained by sticking a droplet (10 μL) of the nanoparticle suspension on a copper grid (200 mesh, covered with Formvar) for 2 min, then removing the droplet with filter paper avoiding the paper touching the grid, then washing twice the grid with a droplet of Milli-Q water for 1 min, and removing the droplet with filter paper. Later, the sample was stained with a solution of 1% phosphotungstic acid by sticking a droplet of this solution on the grid for 2 min and removing the droplet with filter paper. Finally, the grid is allowed to dry for at least 1 h before analysis.

*Sponge Formation.* In order to obtain the solid materials containing PV10, 2 mL of the nanoparticle suspensions showing a $n^+/n^-$ ratio of 0.7 were frozen at −20 °C in a plastic Nunc 24 well plate of 1.6 cm diameter and 1.6 cm depth for 24 h and then liophylized at 0.050 mbar and −57 °C for 72 h. As control experiments, sponges composed of pristine Alg or PSS were formed by freeze-drying 2 mL of $8 \times 10^{-3}$ M polymer solutions as explained above. Assays to obtain sponges from pristine $8 \times 10^{-3}$ M PV10 were not successful, obtaining an agglomerated solid material that was also used as control. SEM images of the sponges were obtained after pouring 1 mL of the colloidal suspensions directly into a well-shaped sample holder matching the equipment characteristics, and then freeze-drying.

*Wafer Formation.* Three sponges of the same composition were stacked and placed between two circular copper plates of 2.4 cm diameter in a sandwich-like configuration (see Figure 2A). The set was gently pressed with the fingers, took with tweezers, and placed on the hollow cylinder base, before screwing. The hollow cylinder was then screwed to the base, keeping the set of sponges inside its lumen. Then, the massive cylinder was introduced by the open end of the hollow cylinder, and 5 tons was applied with the aid of the press for 1 min. The wafers were characterized by the wide-angle XRD method. Samples were measured at 15 rpm in a rotatory holder. XRD


DOI: 10.1021/acs.jpcb.5b05963
J. Phys. Chem. B 2015, 119, 13208−13217

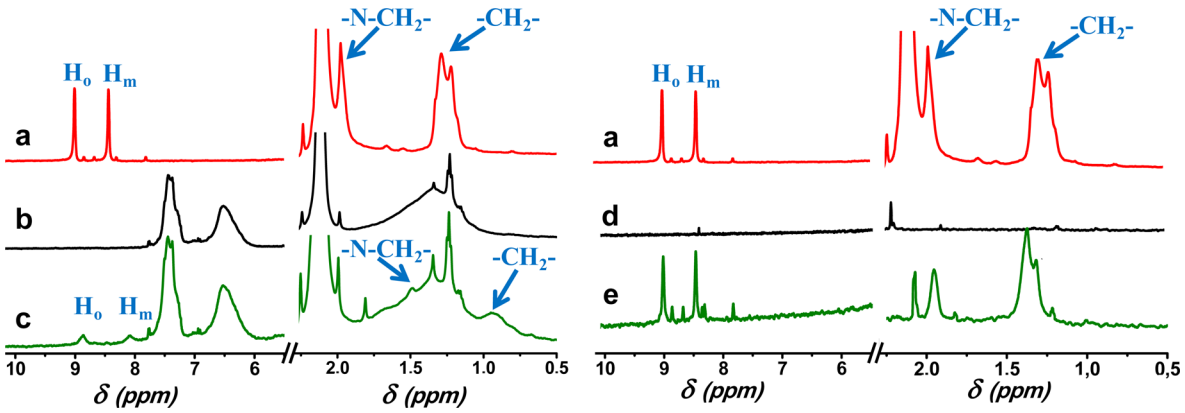


**Figure 3.** The 500 MHz $^1$H NMR spectra in $D_2O$ of solutions containing (a) $1 \times 10^{-3}$ M of PV10, (b) $1 \times 10^{-2}$ M of PSS, (c) $1 \times 10^{-3}$ M of PV10 and $1 \times 10^{-2}$ M of PSS, (d) $1 \times 10^{-2}$ M of Alg, and (e) $1 \times 10^{-3}$ M of PV10 and $1 \times 10^{-2}$ M of Alg.

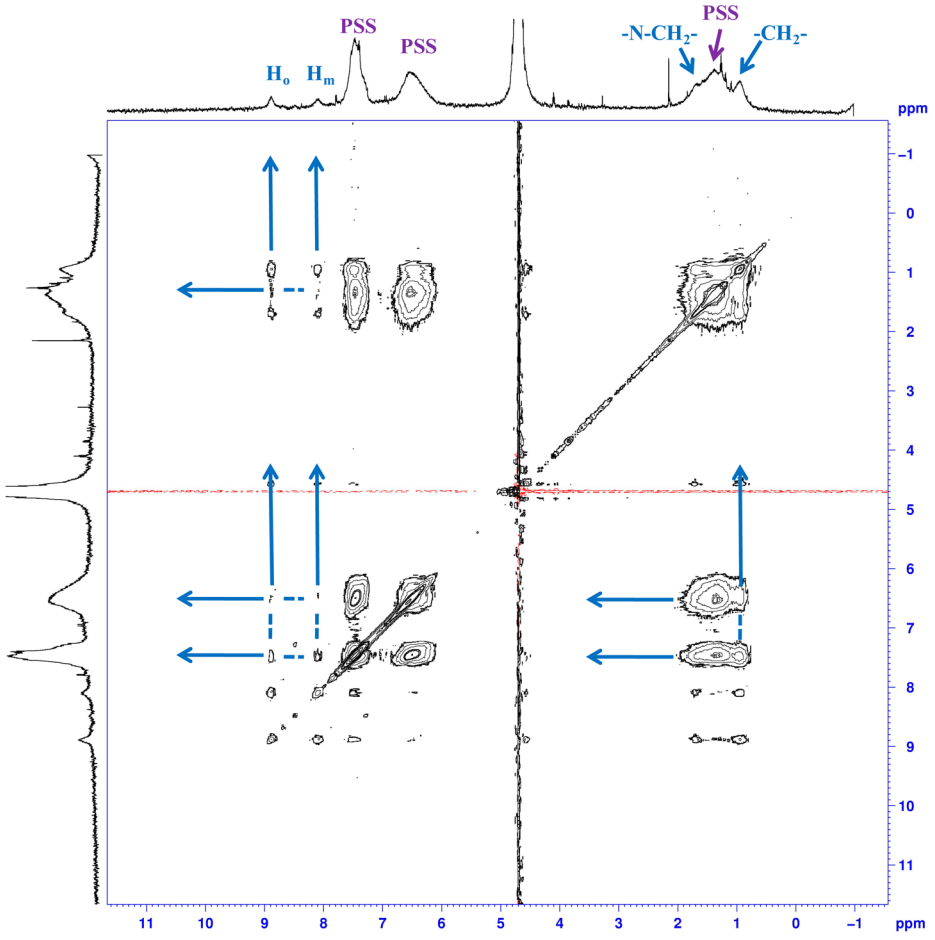


**Figure 4.** The 600 MHz $^1$H NMR NOESY spectrum of solutions containing $1 \times 10^{-3}$ M of PV10 and $1 \times 10^{-2}$ M of PSS in $D_2O$.

patterns were obtained by using radiations of Cu K$\alpha$ ($\lambda$ = 1.54 Å), filtered with Ni at 30 kV and 10 mA, and registered at 2$\theta$ angle between 5° and 80°, with intervals of 2 s each 0.01°. Diffuse reflectance UV−vis spectroscopy was also used to characterize the wafers using $BaSO_4$ as reference standard white. Absorbance data were transformed according to the Kubelka−Munk equation, which correlates the diffuse reflectance with absorption, according to $(1 - R)^2/2R = K/S$, where $R$, $K$, and $S$ are the absolute reflectance of the sampled layer, the molar absorption coefficient, and the scattering coefficient, respectively.

*Wafer Reduction.* Chemical reduction of the wafers was performed by adding one drop of an aqueous solution of $NaBH_4$ ($1 \times 10^{-2}$ M), which was mechanically spread on the wafers, and immediately extracting the excess of liquid with a piece of filter paper. Photochromic responses of the wafers were analyzed by diffuse reflectance UV−vis spectroscopy. Cycles of sun irradiation and discoloration were performed, exposing the samples to direct sunlight during fixed periods of time, and letting them spontaneously decolorize in the dark before submitting to sun irradiation again. Discoloration kinetics were measured immediately after sun irradiation for



DOI: 10.1021/acs.jpcb.5b05963
J. Phys. Chem. B 2015, 119, 13208−13217

2 h. Several spectra were acquired in time keeping the samples in the dark inside the UV−vis spectrometer until complete discoloration was observed.

## 3. RESULTS AND DISCUSSION

**3.1. PV10/Polyanion Interactions.** PSS and Alg present structural differences that may influence the physicochemical properties of the colloidal suspensions and of the resulting sponges. Both polymers show certain rigidity. PSS is a vinyl polymer bearing charged aromatic rings as pendant groups, whereas Alg is a polysaccharide bearing a carboxylate and several hydroxides per monomer unit but does not possess aromatic rings. Since PV10 bears positively charged aromatic rings, aromatic−aromatic interactions between the polyviologen and PSS may be produced in water. Analysis of the observed chemical shifts in NMR experiments appears as a suitable technique to explore the occurrence of aromatic−aromatic interactions. The signals corresponding to aromatic protons of any molecule are commonly affected by the magnetic fields produced by the stacked aromatic rings of other molecules, thus producing upfield shifting of the signals. $^1$H NMR experiments involving PV10/PSS complexes in $D_2O$ show upfield shifting of the PV10 signals in the presence of PSS as polyanion, as can be seen in Figure 3. The ratio polyanion/polycation has been chosen to be 10/1 in order to minimize precipitation (even nanoprecipitation) that should produce losing the signals because of the slow motion of the molecules. The signals assigned to $H_o$ and $H_m$ protons in the bipyridinium moieties (see Figure 1 for assignments) appear at 9.01 and 8.45 ppm for the pristine PV10, and an upfiled shifting of 0.08 and 0.36 ppm is observed in the presence of 10-fold PSS, achieving chemical shifts of 8.92 and 8.09 ppm, respectively. The methylene groups of PV10 are also upfield shifted 0.50 (methylenes bound to the aromatic rings) and 0.33 ppm (aliphatic intra-chain methylenes), achieving values of 1.99 and 1.27 ppm in the absence of PSS and 1.49 and 0.94 ppm, respectively, in the presence of the aromatic counterion. On the contrary, the observed chemical shifts for pristine PV10 are not affected by complexation of the viologen polycation with Alg. The NMR spectrum for the complex PV10/Alg (Figure 3e) shows that the chemical shifts of all aromatic and aliphatic protons are conserved. These observations are in complete agreement with the presence, in addition to long-range electrostatic interactions, of short-range aromatic−aromatic interactions being held in the case of PV10/PSS interpolymer complex, and not in the case of the PV10/Alg complex.

Definite evidence of the occurrence of aromatic−aromatic interactions is given by NOESY experiments. As can be seen in Figure 4, cross-peaks of negative intensity between protons of PV10 and PSS in NOESY experiments appear, indicating that the intermolecular distance falls below 5 Å. No intermolecular NOE effect has been detected in the case of the interaction between PV10 and Alg.

Recently, we have highlighted the importance of aromatic−aromatic interactions[56,57] on the behavior of polyelectrolytes containing charged aromatic rings in the presence of aromatic counterions.[58−64] These interactions have shown to be of potential use for tuning molecular properties of the counterions and to immobilize them on the polymer domain. In the particular case of PSS, in addition to the long-range Coulombic interactions, these short-range aromatic−aromatic interactions have shown to stabilize several systems containing xanthene dyes,[62,65−68] tetrazolium salts,[61] and several drugs.[59] Properties such as luminescent, acid−base, and redox have been tuned by these interactions. For instance, the interaction between PSS and 2,3,5-triphenyl-2*H*-tetrazolium chloride (TTC) results in the stabilization of the cationic, redox-active TTC, decreasing its reduction potential, as seen by cyclic voltammetry experiments.[61]

**3.2. PV10/Polyanion Nanoparticles.** By adequately choosing the total concentration of the solution components and their relative amounts, nanoprecipitates composed of PV10 and the polyanions PSS or Alg were easily obtained. Conditions for the obtention of colloidal nanoparticle suspensions, avoiding macroprecipitation, were searched by fixing the theoretical total amount of polymeric charges at $8 \times 10^{-3}$ M and varying the relative amount of theoretical positive ($n^+$) and negative charges ($n^-$). The results of apparent size and zeta potential are shown in Figure 5 for all the formulations tested.

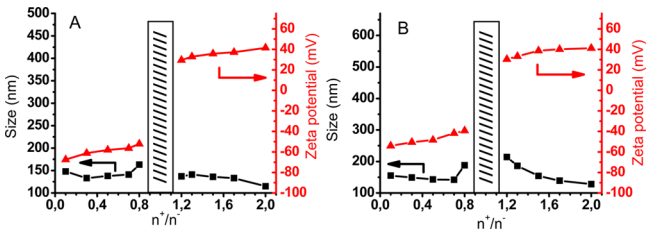


**Figure 5.** Apparent size (hydrodynamic diameter, nm, ■) and zeta potential (mV, red triangle) of the colloidal suspensions as a function of the relative concentration of the polyelectrolytes (A) PV10/PSS and (B) PV10/Alg. Shaded area indicates appearance of macroprecipitates at $n^+/n^- \rightarrow 1.0$.

When the ratio $n^+/n^-$ equals 1 and considering the equivalence on the amount of complementary charges used, macroprecipitates are observed by the naked eye. When the ratio $n^+/n^-$ is equal to or lower than 0.8 or higher than 1.2, colloidal suspensions of nanoparticles showing apparent hydrodynamic diameters of around 150 nm are obtained. For each composition, the nanoparticle suspensions show low polydispersity indexes (PDI), in the range of 0.162−0.090. The zeta potential of the particles takes negative values when the ratio $n^+/n^-$ is lower than 0.8, achieving values lower than −50 mV for PV10/PSS complexes and lower than −30 mV for PV10/Alg complexes. On the contrary, positive values, higher than +30 mV in both cases, were found when the ratio $n^+/n^-$ is higher than 1.2. The values of zeta potential are high enough in absolute value to ensure stability of the suspensions, since repulsions between nanoparticles minimize particle aggregation.

Further studies have been made on formulations containing PV10/PSS and PV10/Alg at an $n^+/n^-$ ratio of 0.7. This composition has been chosen due to the fact that the excess of the polyanion ensures complete complexation of the photochromic PV10. In addition, the suspensions showed nanometric size and low PDI and negative zeta potential whose absolute value is high enough to ensure stability in time. This has been corroborated by checking the size and the zeta potential of the suspensions for 1 week, as can be seen in Figure 6. It can be seen that there is little variation both in the size and the zeta potential of the nanoparticles during this period of time for both formulations.

STEM images obtained after deposition of the colloidal suspensions on Cu grids are shown in Figure 7. The corresponding complexes appeared as particles showing diameters close to those obtained in aqueous suspension.


DOI: 10.1021/acs.jpcb.5b05963
J. Phys. Chem. B 2015, 119, 13208−13217

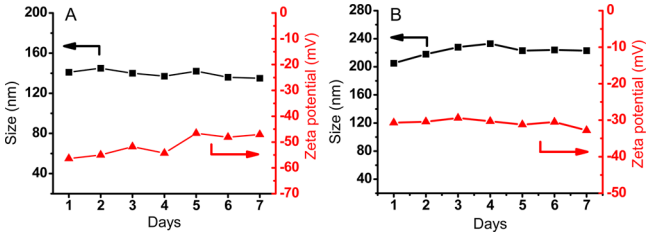


**Figure 6.** Apparent size (hydrodynamic diameter, nm) (■) and zeta potential (mV) (red triangle) of the colloidal suspensions at $n^+/n^-$ ratio of 0.7 as a function of time for (A) PV10/PSS and (B) PV10/Alg.

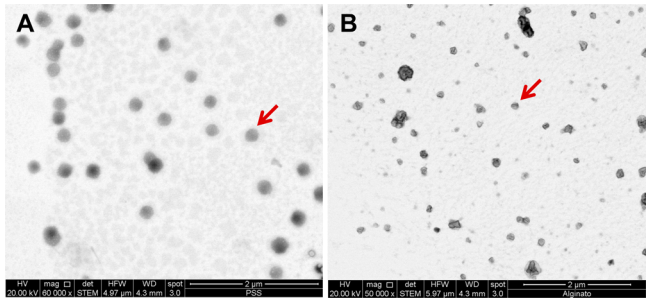


**Figure 7.** STEM images corresponding to (A) PV10/PSS and (B) PV10/Alg. Marked particles show diameters of 219 and 148 nm for (A) and (B), respectively.

However, some differences can be observed comparing both geometry and polydispersion of the particles. The particles obtained from the PV10/PSS complex are more spherical and are less polydisperse than those obtained from the PV10/Alg complex, showing diameters close to 200 nm. Upon aromatic−aromatic interactions, ion pairs may be formed resulting in hydrophobic domains that tend to aggregate. The decamethylene units of PV10 afford higher hydrophobia and the necessary flexibility for PV10 to fold, so that the inner part of the particle may become more fluid, and the surface tension generated at the interface with water forces the particle to adopt a spherical shape. On the contrary, the more hydrophilic Alg produces particles showing a rougher surface, witnessing less surface tension and a higher tendency to spread and agglomerate in a polydisperse way upon solvent evaporation.

**3.3. Sponge Formation.** Sponges with the appearance of sugar-cotton structures were formed by freeze-drying the nanoparticle suspensions of PV10 and PSS or Alg produced considering an $n^+/n^-$ ratio of 0.7. The results can be seen in Figure 8. The sponges had dimensions slightly different from

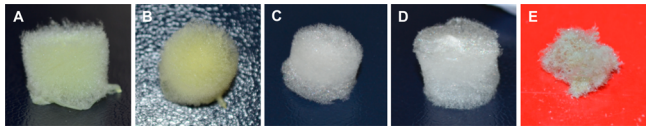


**Figure 8.** Lyophilized samples obtained in well-plates containing: (A) PV10/PSS, (B) PV10/Alg, (C) PSS, (D) Alg, and (E) PV10. The samples showed around 1.5 cm diameter.

those of the volume occupied in the cylindrical container of the well-plates when freezing, contracted in the $x/y$-plane, and expanded in the direction of the $z$-axis. Control sponges of pristine PSS, Alg, and PV10 were successfully obtained in the case of the polyanions, but not in the case of the polycation. Presumably, the low molecular weight of PV10 and its high amphiphilicity and flexibility, related to the decamethylene groups, influence these results. In this respect, complexation with the polyanions furnishes a means of immobilization of the polycation in highly porous materials.

The obtained sponges presented a porous structure made of a combination of micrometric morphologies, such as microfibers and microsheets, showing a high surface area, as can be seen in Figure 9, where SEM images are shown. The solid

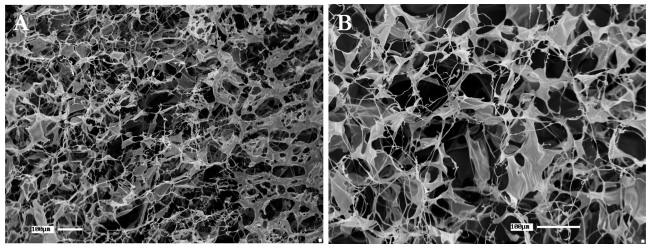


**Figure 9.** SEM images of sponges composed of (A) PV10/PSS and (B) PV10/Alg.

structures seem homogeneous as deduced by the absence of defined textures or agglomerates on their surface. The nanometric size of the formed particles and their low PDI may help to achieve highly homogeneous microfibers and microsheets. Apparently, no significant differences can be seen using PSS or Alg as polyanion. The micrometric complex morphology of the arrangements in these structures in both cases evidences the segregation suffered by the polymeric components by ice during freezing through the ISISA process.

**3.4. Wafer Formation and Photochromism.** Three cylindrical sponges of PV10/PSS, or alternatively of PV10/Alg, of total mass of around 4.5 mg were stacked and pressed in order to obtain circular wafers, similar to starch wafers. As control experiments, wafers made of PSS, or alternatively of Alg, from well-formed sponges were generated by the same method. In addition, the same method was used to obtain wafers of PV10 using the agglomerated mass resulting after freeze-drying. The obtained wafers showed a diameter of around 15 mm, as can be seen in Figure 10.

The wafers were analyzed by XRD. As can be noted in Figure 11, all diffraction patterns present an amorphous halo profile, which is consistent with both the polymeric and microstructured nature of the pressed materials. Nevertheless, it is

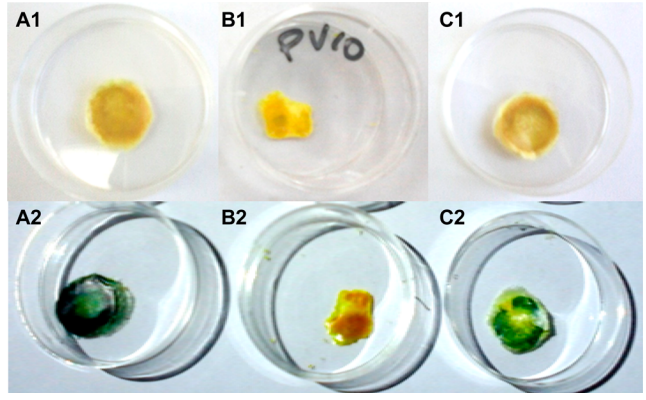


**Figure 10.** Wafers before (X1) and after (X2) exposing to sun irradiation for 6 h. (A*n*) PV10/Alg. (B*n*) pristine PV10. (C*n*) PV10/PSS.



DOI: 10.1021/acs.jpcb.5b05963
J. Phys. Chem. B 2015, 119, 13208−13217

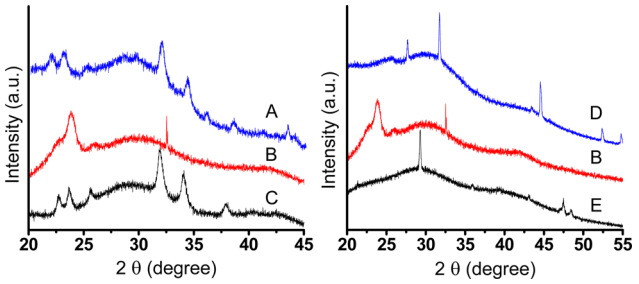


**Figure 11.** XRD patterns of wafers composed of (A) PV10/PSS, (B) PV10, (C) PSS, (D) PV10/Alg, and (E) Alg.

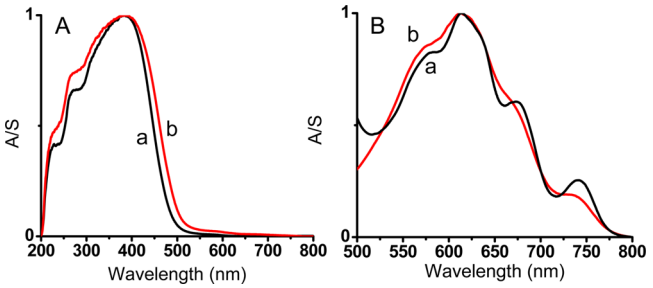


**Figure 12.** Kubelka–Munk absorption spectra for the (A) dication and (B) radical cation states of (a) PV10/PSS and (b) PV10/Alg wafers.

possible to observe in all cases characteristic peaks. PV10 wafers present a broad peak at values of $2\theta$ of around 25°. The calculated distance for the crystalline reflection planes is 3.52 Å. This is a typical distance for $\pi-\pi$ stacking, so that the peak may correspond to self-stacking of the aromatic rings on the solid material, as has been seen in other systems such as in nanofibers of dodecylmethylviologen and coronenes.[69] The diffraction patterns of PV10/PSS and PV10/Alg wafers show the absence of the peak at values of $2\theta$ of around 25°, indicating a change on the configuration of the polycation by complexation with the polyanions, where self-stacking is minimized. PSS wafers present diffraction peaks at 22.7°, 23.6°, 25.6°, 32.0°, 33.0°, and 37.9°. Concerning the diffraction peaks obtained for PV10/PSS wafers, the crystalline structure of PSS is almost conserved, showing a slight shift of the original peaks at 33.0° and 37.9° to 34.5° and 38.6°, respectively, indicating a decrease on the *d*-spacing from 2.71 and 2.37 Å to 2.60 and 2.33 Å, respectively, probably due to contraction and conformational changes of the molecular chains, since electrostatic repulsions are decreased in the presence of the polycation. In addition, other small peaks appear at 36.3°, 41.4°, and 43.6°, corresponding to *d*-spacing of 2.47, 2.18, and 2.08 Å, respectively, revealing the appearance of other diffraction planes upon molecular rearrangement. Alg wafers show diffraction peaks at 29.3°, 47.5°, and 48.5°. When analyzing PV10/Alg wafers, new crystalline peaks appear at 27.6°, 31.6°, 44.6°, and 52.4°. These fine peaks correspond to the formation of cubic NaBr, as corroborated by comparison with available databases (i.e., ICSD 72-1539). Electrostatic interactions between PV10 and Alg allow the respective counterions to diffuse and further crystallize during freeze-drying. It can be noticed that the system PV10/PSS presents a higher ability to disperse these small ions, since the XRD pattern corresponding to NaBr is not found.

Macroscopically, wafers can be seen as pale yellow materials. This is due to the presence of PV10 in its dicationic state, thus oxidized. Absorption spectra of the wafers were obtained by diffuse reflectance, using the known Kubelka–Munk approximation. The corresponding normalized spectra are presented in Figure 12. PV10/PSS and PV10/Alg wafers showed a band centered at 388 nm, consistent with the pale yellow color associated with the dicationic state of PV10, as can be seen in Figure 12A. When the spectra of both types of wafers are compared, no big differences can be found between them. Reduction of the wafers with $NaBH_4$ produced a color change to an intense blue-violet, almost immediately after adding the reducing agent, and witnessed by the appearance of a complex absorption band centered at 614 nm, corresponding to the radical cation, reduced form of PV10, as can be seen in Figure 12B. As well as for the dicationic spectra, no major differences were found, regarding the shape or absorbance maximum, when PV10/PSS and PV10/Alg wafers were compared, although the fine structure of the spectrum is more notorious in the case of PV10/PSS wafers, which may indicate a more rigid configuration for the viologen residue.

The photochromic responses under sun irradiation of both types of wafers have been investigated. Interestingly, PV10/Alg wafers are much more light-sensitive than PV10/PSS. In the case of PV10/Alg wafers, an absorption maximum at 614 nm, corresponding to reduced PV10 species appears, as can be seen in Figure 13 where the different spectra obtained by sun-

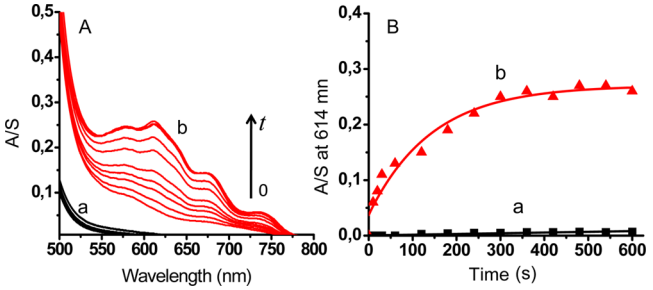


**Figure 13.** (A) Kubelka–Munk absorption spectra for (a) PV10/PSS and (b) PV10/Alg wafers at different *t* (time lapse of 10 min). (B) Photochromic response as a function of *t*, measured for PV10/PSS (a, ■) and PV10/Alg (b, red triangle) at 614 nm. All measurements were performed at 25 °C.

irradiating the samples during different times are shown, together with the corresponding absorbance at 614 nm as a function of time ($t$). It can be seen that a saturation curve is followed for the appearance of the blue color, and the maximum coloration is achieved within the first 5 min. The saturation curve responded to the equation $y = -0.233 \exp(-0.007t) + 0.270$ ($R^2 = 0.96$), where $y$ is the Kubelka–Munk absorbance and $t$ is given in seconds, thus showing a first-order kinetics with a kinetic constant of 0.007 $s^{-1}$. In contrast, a weak photochromic activity was found for PV10/PSS wafers during 3 h of sun irradiation. The slower photochromic responses of PV10/PSS wafers are also qualitatively witnessed after 6 h of sun irradiation, as can be seen in Figure 10.

In addition, total discoloration of the PV10/Alg wafers irradiated for 2 h was found to proceed in the dark in around 2 h, as can be seen in Figure 14, where a decrease on the maximum at 614 nm was observed. The wafers color turned to pale yellow, related to the dicationic state of PV10. The decay of the coloration follows an exponential curve, following the equation $y = 7.3179 \exp(-0.0003t) - 1.018$ ($R^2 = 0.99$), also


DOI: 10.1021/acs.jpcb.5b05963
J. Phys. Chem. B 2015, 119, 13208–13217

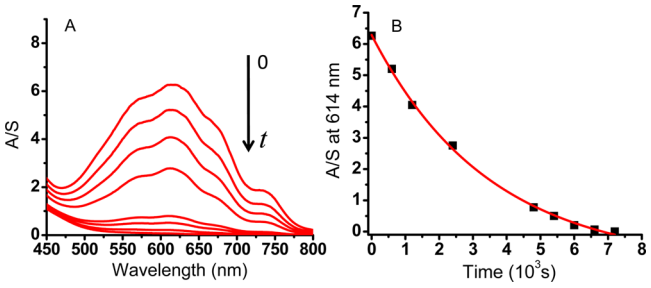


**Figure 14.** (A) Kubelka–Munk absorption spectra for PV10/Alg wafers at different $t$ (time lapse of 120 min). (B) Discoloration kinetics of PV10/Alg (■) measured at 614 nm and 25 °C.

showing a first-order kinetics with a kinetic constant of 0.0003 $s^{-1}$, 1 order of magnitude slower than the coloration process.

**3.5. Final Remarks.** Several studies concerning photochromic materials based on viologens show photochromic responses in the range of days and discoloration in the range of weeks.[1] In this sense, the photochromic responses of PV10/Alg wafers drastically improve these kinetics, since coloration is observed in the order of several minutes, while discoloration is undertaken in the range of several hours in the dark. Interestingly, in PV10/Alg and PV10/PSS sponges and wafers, both the functional polymers responsible for the photochromism as electron acceptor and electron donor, respectively, are at the same time structuring components of the polymeric materials, rather than being embedded in a polymeric matrix of a third component such as PVP.[28] This offers new means of achieving photochromic materials of simpler processability and lower demand of starting materials.

Four basic steps are involved in the fabrication of these materials, each one playing a specific role in the final material properties. The first step is the formation of a colloidal suspension. In this step, the formation of the interpolymer complex is controlled, so that the formation of macroprecipitates is avoided, while enough charge compensation is provided, which facilitates the transfer of an electron from the polyanion to the polycation. The different nature of the intermolecular interactions between PV10 and the respective polyanions may have influence on the phase behavior and molecular arrangement during freezing. The second step is freezing. During this step, formation of ice crystals induces the aggregation and rearrangement of the polymers at the boundary edges of the ice crystal structures. Upon the third step, sublimation of water, a solid, cotton-like porous structure arises. The absence of water allows close contacts between the electron donor and acceptor, making possible the transfer of an electron. The rigidity of the polyanions seems to be a crucial fact to avoid the collapse of the system and maintain the porous structure. The resulting material is light and brittle and shows high effective surface area. The mechanical properties may be improved by pressing several sponges, as the fourth step, in order to obtain wafers as materials with controlled toughness.

Many variables such as nature of the polymers, absolute and relative polymer concentration, working pH and temperature for sponge fabrication, presence or absence of doping agents, humidity, etc., may influence the structure of these materials as well as their photochromic responses. The contrasting photochromic responses observed comparing PV10/Alg and PV10/PSS wafers may be related to the different nature of the interactions involving both oppositely charged polyelectrolytes. Stabilization of the dicationic form of the viologen through aromatic–aromatic interactions with PSS may be a cause of the different photochromic response found between PV10/Alg and PV10/PSS wafers; this stabilization effect should increase the necessary energy to photoreduce the viologen. Photochromic systems based on viologens and benzenesulfonate, such as those formed by the low-molecular-weight molecules *N*,*N*′-diphenyl-4,4′-bipyridinium as photochromic molecule and alkylbenzenesulfonates as electron donor counterions, have shown to be modulated by the length of the alkyl chain in the organic counterion.[32] The molecules arranged in a smectic A-type configuration consisting of intercalated bipyridinium and benzenesulfonate moieties, where aromatic–aromatic interactions play an important role.[28,32] The photoreduction and the corresponding bleaching kinetics are affected by the distances between both molecules, modulated through changes in the length of the alkyl chain of the substituted benzenesulfonate counterions. Longer chains produce an increase on the distance between molecules, consequently decreasing the electron transfer from the counterion to the viologen molecule.[31]

The materials presented here may be optimized by changing any of the variables mentioned above, depending on the application intended. Changes on the polymer relative composition may induce different molecular organization and, thus, produce differences on the photoresponses. The temperature gradient program for freezing may be another variable impacting molecular organization, mechanical stability of the final material, and photochemical properties. The hydrophilic/hydrophobic nature of the polymers also plays an important role, due to the quenching effect on the photoresponse produced by water, as reported in the literature.[27,28] The mechanical properties of the final materials depend on the nature and absolute concentration of the polymeric components in the colloidal suspension, affecting the density and viscoelastic properties, as well as on the pressure applied when fabricating the wafers.

## 4. CONCLUSIONS

Solid materials are obtained by mixing the complementary charged polymers PV10 and PSS or Alg in a charge molar ratio $(n^+/n^-)$ of 0.7, to form nanometric colloidal suspensions, which were submitted to freeze-drying. The colloidal particles showed hydrodynamic diameters of 141 and 142 nm for the complexes PV10/PSS and PV10/Alg, respectively, in narrow size distributions with PDI of 0.091 and 0.096. The zeta potential of these particles took negative values of −56.4 and −41.7 mV, respectively, thus providing stability to the nanoparticles during at least 7 days. The resulting sponges after freeze-drying showed a microporous structure made of microfibers and microsheets. The sponges were pressed to obtain wafers. XRD studies of these materials showed the loose of a peak corresponding to the self-stacking of PV10 aromatic rings, indicating molecular reorganization. Contrasting photochromic responses are observed comparing PV10/PSS and PV10/Alg materials. PV10/Alg wafers showed a fast photochromic response under sun irraditation, a fact that was not observed for PV10/PSS wafers. The photochromic responses of PV10/Alg wafers allowed coloration in the order of minutes, showing a kinetic constant of 0.007 $s^{-1}$, and discoloration in the order of hours, showing a kinetic constant of 0.0003 $s^{-1}$. PSS and PV10 undergo aromatic–aromatic interactions, as seen by $^1$H NMR. The stabilization of the dicationic form of PV10 by means of these interactions may be responsible for the decrease on the kinetics of the photoresponse. These results highlight the


DOI: 10.1021/acs.jpcb.5b05963
J. Phys. Chem. B 2015, 119, 13208–13217

importance of the nature of polymeric counterions of viologens in order to obtain totally polymeric, organic porous materials, with modulable coloration−discoloration photoreaction kinetics, easy processability, and low demand of starting materials.

## AUTHOR INFORMATION


### Corresponding Author

*E-mail: imorenovilloslada@uach.cl (I.M.-V.).


### Notes

The authors declare no competing financial interest.

## ACKNOWLEDGMENTS

This work was supported by FONDECYT Postdoctorado No. 3140221 and FONDECYT Regular 1050899, FONDAP 15130011, and Basal Financing Program, Conicyt, No. FB0807 (CEDENNA). We acknowledge the support of Waseda Advanced Research Institute for Science & Engineering.

## REFERENCES


(1) Lin, R. G.; Xu, G.; Wang, M. S.; Lu, G.; Li, P. X.; Guo, G. C. Improved Photochromic Properties on Viologen-Based Inorganic-Organic Hybrids by Using Π-Conjugated Substituents as Electron Donors and Stabilizers. *Inorg. Chem.* **2013**, *52*, 1199−1205.

(2) Ungashe, S. B.; Wilson, W. L.; Katz, H. E.; Scheller, G. R.; Putvinski, T. M. Synthesis, Self-Assembly, and Photophysical Dynamics of Stacked Layers of Porphyrin and Viologen Phosphonates. *J. Am. Chem. Soc.* **1992**, *114*, 8717−8719.

(3) Peon, J.; Tan, X.; Hoerner, J. D.; Xia, C.; Luk, Y. F.; Kohler, B. Excited State Dynamics of Methyl Viologen. Ultrafast Photoreduction in Methanol and Fluorescence in Acetonitrile. *J. Phys. Chem. A* **2001**, *105*, 5768−5777.

(4) Bird, C. L.; Kuhn, A. T. Electrochemistry of the Viologens. *Chem. Soc. Rev.* **1981**, *10*, 49−82.

(5) De Long, H. C.; Buttry, D. A. Ionic Interactions Play a Major Role in Determining the Electrochemical Behavior of Self-Assembling Viologen Monolayers. *Langmuir* **1990**, *6*, 1319−1322.

(6) Garcia-Cañadas, J.; Fabregat-Santiago, F.; Kapla, J.; Bisquert, J.; Garcia-Belmonte, G.; Mora-Seró, I.; Edwards, M. O. M. Dynamic Behaviour of Viologen-Activated Nanostructured $TiO_2$: Correlation between Kinetics of Charging and Coloration. *Electrochim. Acta* **2004**, *49*, 745−752.

(7) Sano, N.; Tomita, W.; Hara, S.; Min, C. M.; Lee, J. S.; Oyaizu, K.; Nishide, H. Polyviologen Hydrogel with High-Rate Capability for Anodes toward an Aqueous Electrolyte-Type and Organic-Based Rechargeable Device. *ACS Appl. Mater. Interfaces* **2013**, *5*, 1355−1361.

(8) Anandan, S. Viologen Impregnated Pvdf with $TiO_2$ Nanofiller as a Solid Polymer Electrolyte for Dye-Sensitized Solar Cells. *Curr. Appl. Phys.* **2008**, *8*, 99−103.

(9) Sano, N.; Suzuki, M.; Tomita, W.; Oyaizu, K.; Nishide, H. Indoline Dye-Coupled Polyviologen: Its Electrochemical Property and Electropolymerization. *Jpn. J. Appl. Phys.* **2012**, *51*, 10NE17.

(10) Sharma, G. D.; Sharma, S.; Roy, M. S. Electrical and Photoelectrical Properties of Dye-Sensitized Allyl Viologen-Doped Polypyrrole Solar Cells. *Sol. Energy Mater. Sol. Cells* **2003**, *80*, 131−142.

(11) DeLongchamp, D. M.; Kastantin, M.; Hammond, P. T. High-Contrast Electrochromism from Layer-by-Layer Polymer Films. *Chem. Mater.* **2003**, *15*, 1575−1586.

(12) Takahashi, Y.; Hayashi, N.; Oyaizu, K.; Honda, K.; Nishide, H. Totally Organic Polymer-Based Electrochromic Cell Using Tempo-Substituted Polynorbornene as a Counter Electrode-Active Material. *Polym. J.* **2008**, *40*, 763−767.

(13) Schlenoff, J. B.; Laurent, D.; Ly, H.; Stepp, J. Redox-Active Polyelectrolyte Multilayers. *Adv. Mater.* **1998**, *10*, 347−349.

(14) Bhowmik, P. K.; Han, H.; Cebe, J. J.; Burchett, R. A.; Sarker, A. M. Main-Chain Viologen Polymers with Organic Counterions Exhibiting Thermotropic Liquid-Crystalline and Fluorescent Properties. *J. Polym. Sci., Part A: Polym. Chem.* **2002**, *40*, 659−674.

(15) Zotti, G.; Zecchin, S.; Vercelli, B.; Berlin, A.; Grimoldi, S.; Bertoncello, R.; Milanese, L. Self-Assembled Monolayers and Electrostatically Self-Assembled Multilayers of Polyalkylviologens on Sulfonate-Modified Gold and Indium−Tin−Oxide Electrodes. *J. Electroanal. Chem.* **2005**, *580*, 330−339.

(16) Amao, Y.; Shuto, N. Formate Dehydrogenase−Viologen-Immobilized Electrode for $CO_2$ Conversion, for Development of an Artificial Photosynthesis System. *Res. Chem. Intermed.* **2014**, *40*, 3267−3276.

(17) Pan, Y.; Stockton, J.; Urie, R.; Pitt, W.; Wheeler, D. R. Immobilized Viologen Polymers for Carbohydrate Fuel Cells. *ECS Trans.* **2013**, *50*, 819−828.

(18) Kamogawa, H.; Suzuki, T. Organic Solid Photochromism Via a Photoreduction Mechanism. Photochromism of Viologen Crystals. *J. Chem. Soc., Chem. Commun.* **1985**, 525−526.

(19) Sampanthar, J. T.; Neoh, K. G.; Ng, S. W.; Kang, E. T.; Tan, K. L. Flexible Smart Window Via Surface Graft Copolymerization of Viologen on Polyethylene. *Adv. Mater.* **2000**, *12*, 1536−1539.

(20) Crano, J. C.; Guglielmetti, R. J. *Organic Photochromic and Thermochromic Compounds*; Springer: New York, 2006; Vol. 2.

(21) Xu, G.; Guo, G.-C.; Guo, J.-S.; Guo, S.-P.; Jiang, X.-M.; Yang, C.; Wang, M.-S.; Zhang, Z.-J. Photochromic Inorganic-Organic Hybrid: A New Approach for Switchable Photoluminescence in the Solid State and Partial Photochromic Phenomenon. *Dalton Trans.* **2010**, *39*, 8688−8692.

(22) Xu, G.; Guo, G.-C.; Wang, M.-S.; Zhang, Z.-J.; Chen, W.-T.; Huang, J.-S. Photochromism of a Methyl Viologen Bismuth(III) Chloride: Structural Variation before and after Uv Irradiation. *Angew. Chem., Int. Ed.* **2007**, *46*, 3249−3251.

(23) Lee, P. C.; Matheson, M. S.; Meisel, D. Photogeneration of Hydrogen from Polymeric Viologen Systems. *Isr. J. Chem.* **1982**, *22*, 133−137.

(24) Gong, Y.-N.; Lu, T.-B. Fast Detection of Oxygen by the Naked Eye Using a Stable Metal-Organic Framework Containing Methyl Viologen Cations. *Chem. Commun.* **2013**, *49*, 7711−7713.

(25) Li, P.-X.; Wang, M.-S.; Zhang, M.-J.; Lin, C.-S.; Cai, L.-Z.; Guo, S.-P.; Guo, G.-C. Electron-Transfer Photochromism to Switch Bulk Second-Order Nonlinear Optical Properties with High Contrast. *Angew. Chem., Int. Ed.* **2014**, *53*, 11529−11531.

(26) Kamogawa, H.; Kikushima, K.; Nanasawa, M. Photomemory of Viologen Copolymers. *J. Polym. Sci., Part A: Polym. Chem.* **1989**, *27*, 393−396.

(27) Kamogawa, H.; Masui, T.; Nanasawa, M. Photochemically Induced Reduction of Viologens in Solid Polar Aprotic Polymer Matrices. *Chem. Lett.* **1980**, *9*, 1145−1148.

(28) Nanasawa, M. Photochromism by Electron Transfer: 'Photochromic Viologens'. In *Organic Photochromic and Thermochromic Compounds*; Crano, J., Guglielmetti, R., Eds.; Springer: New York, 2002; pp 341−369.

(29) Nanasawa, M.; Miwa, M.; Hirai, M.; Kuwabara, T. Synthesis of Viologens with Extended Π−Conjugation and Their Photochromic Behavior on near-Ir Absorption. *J. Org. Chem.* **2000**, *65*, 593−595.

(30) Haramoto, Y.; Yin, M.; Matukawa, Y.; Ujiie, S.; Nanasawa, M. A New Ionic Liquid Crystal Compound with Viologen Group in the Principal Structure. *Liq. Cryst.* **1995**, *19*, 319−320.

(31) Kamogawa, H.; Ono, T. Redox Photochromism in Films of Viologens and Related Compounds Bearing Long-Chain Alkyl Groups. *Chem. Mater.* **1991**, *3*, 1020−1023.

(32) Nanasawa, M.; Matsukawa, Y.; Jin, J. J.; Haramoto, Y. Redox Photochromism of Viologen in Organized Solid State. *J. Photochem. Photobiol., A* **1997**, *109*, 35−38.

(33) Kamogawa, H.; Nanasawa, M. Effect of Temperature on the Color Developed by near Ultraviolet Light for 4,4′-Bipyridinium Salts (Viologens) Embedded in Poly(1-Vinyl-2-Pyrrolidone) Matrix. *Bull. Chem. Soc. Jpn.* **1993**, *66*, 2443−2445.




DOI: 10.1021/acs.jpcb.5b05963
J. Phys. Chem. B 2015, 119, 13208−13217

(34) Sun, J.-K.; Wang, P.; Yao, Q.-X.; Chen, Y.-J.; Li, Z.-H.; Zhang, Y.-F.; Wu, L.-M.; Zhang, J. Solvent- and Anion-Controlled Photochromism of Viologen-Based Metal-Organic Hybrid Materials. *J. Mater. Chem.* **2012**, *22*, 12212−12219.
(35) Zeng, Y.; Liao, S.; Dai, J.; Fu, Z. Fluorescent and Photochromic Bifunctional Molecular Switch Based on a Stable Crystalline Metal-Viologen Complex. *Chem. Commun.* **2012**, *48*, 11641−11643.
(36) Kuwabara, T.; Sugiyama, M.; Nanasawa, M. Photochromism of Viologens Included in Crown Ether Cavity. *Photochem. Photobiol.* **2001**, *73*, 469−472.
(37) Mourtzis, N.; Carballada, P. C.; Felici, M.; Nolte, R. J. M.; Williams, R. M.; de Cola, L.; Feiters, M. C. Cyclodextrin-Based Systems for Photoinduced Hydrogen Evolution. *Phys. Chem. Chem. Phys.* **2011**, *13*, 7903−7909.
(38) Kuwabara, T.; Sugiyama, M.; Takeuchi, K.; Sakane, H. Catenane and Inclusion Complex as Photochromic Compounds Involving Viologen Units. *J. Photochem. Photobiol., A* **2013**, *269*, 59−64.
(39) Nagamura, T.; Sakaguchi, H.; Muta, S.; Ito, T. Ultrafast Photon-Mode Recording by Novel Photochromic Polymer Via Photoinduced Electron Transfer. *Appl. Phys. Lett.* **1993**, *63*, 2762−2764.
(40) Yoon, K. B.; Kochi, J. K. Direct Observation of Superoxide Electron Transfer with Viologens by Immobilization in Zeolite. *J. Am. Chem. Soc.* **1988**, *110*, 6586−6588.
(41) Li, H.-Y.; Wei, Y.-L.; Dong, X.-Y.; Zang, S.-Q.; Mak, T. C. W. Novel Tb-Mof Embedded with Viologen Species for Multi-Photofunctionality: Photochromism, Photomodulated Fluorescence, and Luminescent Ph Sensing. *Chem. Mater.* **2015**, *27*, 1327−1331.
(42) Wu, J.; Tao, C.; Li, Y.; Li, J.; Yu, J. Methyl Viologen-Templated Zinc Gallophosphate Zeolitic Material with Dual Photo-/Thermochromism and Tuneable Photovoltaic Activity. *Chemical Science* **2015**, *6*, 2922−2927.
(43) Gutiérrez, M. C.; Ferrer, M. L.; del Monte, F. Ice-Templated Materials: Sophisticated Structures Exhibiting Enhanced Functionalities Obtained after Unidirectional Freezing and Ice-Segregation-Induced Self-Assembly. *Chem. Mater.* **2008**, *20*, 634−648.
(44) Zhang, X.; Li, C.; Luo, Y. Aligned/Unaligned Conducting Polymer Cryogels with Three-Dimensional Macroporous Architectures from Ice-Segregation-Induced Self-Assembly of Pedot-Pss. *Langmuir* **2011**, *27*, 1915−1923.
(45) Zhang, H.; Hussain, I.; Brust, M.; Butler, M. F.; Rannard, S. P.; Cooper, A. I. Aligned Two- and Three-Dimensional Structures by Directional Freezing of Polymers and Nanoparticles. *Nat. Mater.* **2005**, *4*, 787−793.
(46) Madihally, S. V.; Matthew, H. W. T. Porous Chitosan Scaffolds for Tissue Engineering. *Biomaterials* **1999**, *20*, 1133−1142.
(47) Gutiérrez, M. C.; Jobbágy, M.; Rapún, N.; Ferrer, M. L.; Del Monte, F. A Biocompatible Bottom-up Route for the Preparation of Hierarchical Biohybrid Materials. *Adv. Mater.* **2006**, *18*, 1137−1140.
(48) Stepp, J.; Schlenoff, J. B. Electrochromism and Electrocatalysis in Viologen Polyelectrolyte Multilayers. *J. Electrochem. Soc.* **1997**, *144*, L155−L158.
(49) Chen, S. C.; Wu, Y. C.; Mi, F. L.; Lin, Y. H.; Yu, L. C.; Sung, H. W. A Novel Ph-Sensitive Hydrogel Composed of N,O-Carboxymethyl Chitosan and Alginate Cross-Linked by Genipin for Protein Drug Delivery. *J. Controlled Release* **2004**, *96*, 285−300.
(50) Madziva, H.; Kailasapathy, K.; Phillips, M. Evaluation of Alginate-Pectin Capsules in Cheddar Cheese as a Food Carrier for the Delivery of Folic Acid. *LWT - Food Sci. Technol.* **2006**, *39*, 146−151.
(51) Hari, P. R.; Chandy, T.; Sharma, C. P. Chitosan/Calcium−Alginate Beads for Oral Delivery of Insulin. *J. Appl. Polym. Sci.* **1996**, *59*, 1795−1801.
(52) Rowley, J. A.; Madlambayan, G.; Mooney, D. J. Alginate Hydrogels as Synthetic Extracellular Matrix Materials. *Biomaterials* **1999**, *20*, 45−53.
(53) Zimmermann, H.; Shirley, S. G.; Zimmermann, U. Alginate-Based Encapsulation of Cells: Past, Present, and Future. *Curr. Diabetes Rep.* **2007**, *7*, 314−320.
(54) Zhang, Z.; Zhang, R.; Decker, E. A.; McClements, D. J. Development of Food-Grade Filled Hydrogels for Oral Delivery of Lipophilic Active Ingredients: Ph-Triggered Release. *Food Hydrocolloids* **2015**, *44*, 345−352.
(55) Adeogun, M. J.; Hay, J. N. Silica−Polyviologen Hybrids Prepared by the Sol−Gel Route. 1. Synthesis and Thermal Characterisation of Ionene Systems. *Polym. Int.* **1996**, *41*, 123−134.
(56) Hunter, C. A.; Sanders, J. K. M. The Nature Of.Pi.-.Pi. Interactions. *J. Am. Chem. Soc.* **1990**, *112*, 5525−5534.
(57) Meyer, E. A.; Castellano, R. K.; Diederich, F. Interactions with Aromatic Rings in Chemical and Biological Recognition. *Angew. Chem., Int. Ed.* **2003**, *42*, 1210−1250.
(58) Nordmeier, E. Advances in Polyelectrolyte Research: Counterion Binding Phenomena, Dynamic Processes, and the Helix-Coil Transition of DNA. *Macromol. Chem. Phys.* **1995**, *196*, 1321−1374.
(59) Moreno-Villoslada, I.; González, F.; Rivas, B. L.; Shibue, T.; Nishide, H. Tuning the Pka of the Antihistaminic Drug Chlorpheniramine Maleate by Supramolecular Interactions with Water-Soluble Polymers. *Polymer* **2007**, *48*, 799−804.
(60) Moreno-Villoslada, I.; Jofré, M.; Miranda, V.; González, R.; Sotelo, T.; Hess, S.; Rivas, B. L. Ph Dependence of the Interaction between Rhodamine B and the Water-Soluble Poly(Sodium 4-Styrenesulfonate). *J. Phys. Chem. B* **2006**, *110*, 11809−11812.
(61) Moreno-Villoslada, I.; Soto, M.; González, F.; Montero-Silva, F.; Hess, S.; Takemura, I.; Oyaizu, K.; Nishide, H. Reduction of 2,3,5-Triphenyl-2h-Tetrazolium Chloride in the Presence of Polyelectrolytes Containing 4-Styrenesulfonate Moieties. *J. Phys. Chem. B* **2008**, *112*, 5350−5354.
(62) Moreno-Villoslada, I.; Torres-Gallegos, C.; Araya-Hermosilla, R.; Nishide, H. Influence of the Linear Aromatic Density on Methylene Blue Aggregation around Polyanions Containing Sulfonate Groups. *J. Phys. Chem. B* **2010**, *114*, 4151−4158.
(63) Toncelli, C.; Pino-Pinto, J. P.; Sano, N.; Picchioni, F.; Broekhuis, A. A.; Nishide, H.; Moreno-Villoslada, I. Controlling the Aggregation of 5,10,15,20-Tetrakis-(4-Sulfonatophenyl)-Porphyrin by the Use of Polycations Derived from Polyketones Bearing Charged Aromatic Groups. *Dyes Pigm.* **2013**, *98*, 51−63.
(64) Gómez-Tardajos, M.; Pino-Pinto, J. P.; Díaz-Soto, C.; Flores, M. E.; Gallardo, A.; Elvira, C.; Reinecke, H.; Nishide, H.; Moreno-Villoslada, I. Confinement of 5,10,15,20-Tetrakis-(4-Sulfonatophenyl)-Porphyrin in Novel Poly(Vinylpyrrolidone)S Modified with Aromatic Amines. *Dyes Pigm.* **2013**, *99*, 759−770.
(65) Araya-Hermosilla, R.; Araya-Hermosilla, E.; Torres-Gallegos, C.; Alarcón-Alarcón, C.; Moreno-Villoslada, I. Sensing Cu2+ by Controlling the Aggregation Properties of the Fluorescent Dye Rhodamine 6g with the Aid of Polyelectrolytes Bearing Different Linear Aromatic Density. *React. Funct. Polym.* **2013**, *73*, 1455−1463.
(66) Araya-Hermosilla, E.; Muñoz, D.; Orellana, S.; Yáñez, A.; Olea, A. F.; Oyarzun-Ampuero, F.; Moreno-Villoslada, I. Immobilization of Rhodamine 6g in Calcium Alginate Microcapsules Based on Aromatic−Aromatic Interactions with Poly(Sodium 4-Styrenesulfonate). *React. Funct. Polym.* **2014**, *81*, 14−21.
(67) Fuenzalida, J. P.; Flores, M. E.; Móniz, I.; Feijoo, M.; Goycoolea, F.; Nishide, H.; Moreno-Villoslada, I. Immobilization of Hydrophilic Low Molecular-Weight Molecules in Nanoparticles of Chitosan/Poly(Sodium 4-Styrenesulfonate) Assisted by Aromatic−Aromatic Interactions. *J. Phys. Chem. B* **2014**, *118*, 9782−9791.
(68) Moreno-Villoslada, I.; González, R.; Hess, S.; Rivas, B. L.; Shibue, T.; Nishide, H. Complex Formation between Rhodamine B and Poly(Sodium 4-Styrenesulfonate) Studied by 1h-Nmr. *J. Phys. Chem. B* **2006**, *110*, 21576−21581.
(69) Mogera, U.; Sagade, A. A.; George, S. J.; Kulkarni, G. U. Ultrafast Response Humidity Sensor Using Supramolecular Nanofibre and Its Application in Monitoring Breath Humidity and Flow. *Sci. Rep.* **2014**, *4*, 4103.


DOI: 10.1021/acs.jpcb.5b05963
*J. Phys. Chem. B* 2015, 119, 13208−13217